INCORPORATING GENERAL RACE AND HOUSING FLEXIBILITY AND DEADBAND IN ROLLING ELEMENT BEARING ANALYSIS*

R.R. Davis and C.S. Vallance
Aerojet TechSystems Company
P.O. Box 13222
Sacramento, California 95813, U.S.A.

New methods for including the effects of general race and housing compliance and outer race-to-housing deadband (clearance) in rolling element bearing mechanics analysis is presented. It is shown that these effects can cause significant changes in bearing stiffness characteristics, which are of major importance in rotordynamic response of turbomachinery and other rotating systems. Preloading analysis is demonstrated with the new finite element/contact mechanics hybrid method applied to a 45 mm angular contact ball bearing.

INTRODUCTION

Accurate analytical prediction of the rotordynamic performance of turbomachinery has foremost dependence on accurate knowledge of the stiffness of bearings and bearing support components. Classical methods of rolling element bearing loading analysis developed by Jones [1] and Harris [2] have proven quite useful in cases where the inherent race rigidity assumption (except local contact deformation) is reasonable. However, critical speed and rotordynamic stability predictions for turbomachinery using these techniques are often inaccurate. Comparisons with test data usually indicate that the predicted bearing stiffness is too high, sometimes by large factors which have eluded quantitative explanation.

Most conventional turbomachinery using angular contact ball bearings has outer race clearance or deadband to accommodate radial growth and axial movement of the shaft assembly in response to thermal or thrust balance forces. The presence of deadband violates the classical assumption of race rigidity because the outer race is allowed to deform within the clearance annulus when the bearing is loaded. The result is a reduction of bearing stiffness as seen by the rotor, and nonlinearity introduced by the clearance gap.

Despite the possible importance of the aforementioned effects on rotordynamic behavior, they have not received significant attention in the literature. Kleckner, Pirvics, and Castelli [3] have included radial housing and simplified race compliance as influence coefficients in their high capability software CYBEAN and SPHERBEAN, but discussion centered on thermal and other effects pertinent to bearing internal motions only. Childs and Moyer [4], among others, have simulated the bearing deadband effect on rotordynamics and have shown that it can cause resonance frequency shifts and subsynchronous response. However, no one known to the authors has documented in detail the effect of race flexibility. In fact, it is largely ignored even today in very comprehensive turbomachinery bearing investigations such as described in reference [5]. Bearing stiffness testing is often done by back-calculation from shaft critical speeds for lack of confidence in predicted values. For example, see the work of Beatty [6]. These tests may be subject to significant error, as critical speeds depend on other factors that may be difficult to accurately control or model. Furthermore, deadband and bearing stiffness effects are not separable in these tests, leading to questionable results.

This work will expand on the analysis of [3] to describe in detail new methods to incorporate general housing and race flexibility models, including deadband, in the mechanics of rolling element bearing loading. The techniques will be developed in the context of angular contact bearings only in the interest of brevity;

*This work was supported by company IR&D funding at Aerojet TechSystems Company, Sacramento, California, project number NLRDA6, and is approved for public release.

C.5

extension to other bearing types is analogous. The objective is to provide straightforward tools to better address the stiffness characteristics of rolling element bearings in rotordynamic analysis. The results are applicable to bearing life evaluation and dynamics as well. Discussion will begin with qualitative description of flexibility and deadband effects. The methods will be developed mathematically, and then demonstrated for bearing preload analysis. General bearing loading examples are extensive and will appear in a separate paper.

NOMENCLATURE

BD	:	Unloaded distance between curvature centers, (m)
c	:	Radial deadband, (m)
c_{ij}, c_{irj}, c_{izj}	:	Inner race component Hertzian contact compliance, (m/N)
c_{oj}, c_{orj}, c_{ozj}	:	Outer race component Hertzian contact compliance, (m/N)
$\mathbf{C}$	:	Total bearing tangent compliance matrix, (m/N)
$\mathbf{C}_i$, $\mathbf{C}_o$	:	Race ball contact tangent compliance matrices, (m/N)
$\mathbf{C}_{rr}$, etc.	:	Partitions of race compliance matrix, (m/N)
d_m	:	Bearing pitch diameter, (m)
D	:	Ball diameter, (m)
f_i, f_o	:	Raceway osculations
F_r, F_θ	:	External loads on bearing along r, θ, (N)
F_{rk}, F_{zk}	:	Radial and axial loads at deadband gap k, (N)
k_r, k_z	:	Gap closure stiffnesses, (N/m)
K	:	Contact stiffness parameters, ($N/m^{1.5}$)
$\mathbf{K}_i$, $\mathbf{K}_o$	:	Bearing race stiffness matrix, (N/m)
K_{ij}, K_{oj}	:	Contact stiffness parameters at ball j, ($N/m^{1.5}$)
$\mathbf{K}_{oo}$, etc.	:	Partitions of race stiffness matrix, (N/m)
KL0, KL1, KL2, KL3	:	Configuration labels
ℓ_{1j}, ℓ_{2j}	:	Ball load lever arms for inner race, ball j, (m)
Q	:	Ball load, (N)
Q_{ij}, Q_{oj}	:	Ball loads at ball j, (N)
Q_{irj}, Q_{izj}	:	Inner race component ball loads at ball j, (N)
Q_{orj}, Q_{ozj}	:	Outer race component ball loads at ball j, (N)
r, θ	:	Radial and lateral coordinate directions
r_{hk}, z_{hk}	:	Housing deflections at gap k, (m)
r_{ij}, z_{ij}	:	Radial and axial inner race deflection at ball j contact, (m)
r_{oj}, z_{oj}	:	Radial and axial outer race deflection at ball j contact, (m)
r_{rk}, z_{rk}	:	Outer race outer surface deflection at gap k, (m)
$\mathscr{R}_i$, $\mathscr{R}_o$	:	Radii to raceway curvature centers, (m)
u_r, u_θ	:	Inner race deflections along r, θ, (m)
x, y, z	:	Cartesian axes, z axial
$\mathscr{F}_i$	:	Inner race axial offset from load application point to curvature center locus, (m)
α°	:	Unloaded contact angle, (rad)
α_{ij}, α_{oj}	:	Contact angles, (rad)
$\Delta\mathbf{F}_x$	:	Vector of ΔQ_{irj}, ΔQ_{izj}
$\Delta\mathbf{F}_\delta$	:	Resultant load error vector
ΔQ_{ij}, ΔQ_{oj}	:	Incremental ball loads at ball j, (N)
Δr_{bj}, Δz_{bj}	:	Δr_j, Δz_j augmented by race deflection contributions, (m)

Δr_j, Δz_j	:	Radial and axial ball contact deflections due to inner race rigid body displacements, (m)
Δr_{oj}, Δz_{oj}	:	Incremental versions of r_{oj}, z_{oj}, (m)
$\Delta \mathbf{x}$	:	Vector of Δr_j, Δz_j
$\Delta \mathbf{x}_h$	:	Incremental housing deflection, (m)
$\Delta \mathbf{x}_r$	:	Incremental outer race outer surface deflection, (m)
ε_{oh}, etc.	:	Partitions of race stiffness matrix due to gap stiffness, (N/m)
θ_x, θ_y	:	Total or incremental rigid body rotations of inner race, (m)
Λ_F	:	Resultant load summation matrix
Λ_δ	:	Inner race kinematic transformation matrix
δ	:	Contact deflection, (m)
$\boldsymbol{\delta}$	:	Vector of δ_x, δ_y, δ_a, θ_x, θ_y
δ_{ij}, δ_{oj}	:	Hertzian contact deflections at ball j, (m)
δ_{irj}, δ_{izj}	:	Inner race component Hertzian contact deflections at ball j, (m)
δ_{orj}, δ_{ozj}	:	Outer race component Hertzian contact deflections at ball j, (m)
δ_x, δ_y, δ_a	:	Total or incremental rigid body translations of inner race, (m)
ψ_j	:	Ball azimuth angle from Cartesian x, (rad)
$(\ )^T$	:	Transpose
$(\ )^{-1}$	:	Inverse
$(\ )_o$	:	Outer race
$(\ )_i$	:	Inner race
$(\ )_j$	:	Ball index
$(\ )_k$	:	Gap index
$(\ )_{rk}$	:	Pertaining to outer race outer surface at gap k
$(\ )_{hk}$	:	Pertaining to housing at gap k

EFFECTS OF RACE/HOUSING FLEXIBILITY AND DEADBAND

The reduction of bearing stiffness due to outer race freedom has already been mentioned in general terms, and some discussion in the context of roller bearings and simple thin ring assumptions can be found in [2], Chapter 6.11. Outer race bulk deformation can cause redistribution of ball loads within the bearing and change in stiffness characteristics. Besides reduction of bearing axial and radial stiffness, asymmetry of stiffness also results as a by-product of the deadband. Referring to Figure 1, deadband allows the outer race to roll along the housing bore surface in response to load. As a result, the stiffness of the bearing in the direction lateral to contact, θ in Figure 1, may be much smaller than in the contact direction r. In the case of zero contact load, the θ stiffness is in fact zero, while the r stiffness is some finite value in compression. For non-zero load along r, the θ stiffness is greater than zero due to development of a contact area by race bulk deformation that can resist moments. Figure 2 shows the general load-deflection relationships for a given preload system. In rotordynamic analysis, this data would be used in two different ways:

1. Large Steady Radial Load - If steady radial loads exist to hold the rotor and bearing against the bore, the slope of the curves for F_r given and $F_\theta = 0$ could be used as linear stiffness for small perturbation modal, imbalance harmonic, or transient analysis. In this case, bearing stiffness is very asymmetric, in fixed directions.

2. Small Steady Radial Load - In this case, deadband nonlinearity must be included in transient analysis. Bearing stiffness in conjunction with deadband can be modeled using the radial load-deflection curve only and instantaneous shaft/housing position which can be expressed in r only. The rolling effect is then implicit and bearing stiffness changes in magnitude and direction in proper response to shaft motion.

It is important to note that deadband itself has its own effects on rotordynamics separate from the induced bearing stiffness reduction. Clearance can lead to impact phenomena and complicated response, which will not be discussed in detail here. Clearance has been shown [4] to reduce critical speeds just as a softer bearing would, so the effects are not readily separable unless one carefully quantifies the true stiffness reduction first. The objective is thus to accurately determine the curves of Figure 2 to be used in rotordynamic analysis. Housing/race flexibility and gap closure will determine the shape of the curves, along with the nonlinear Hertzian contact between the rolling elements and the races, described by

$$Q = K\delta^{3/2} \tag{1}$$

NEW FINITE ELEMENT/CONTACT MECHANICS METHOD

Approach

Finite element modeling is readily available and allows general modeling capability, including arbitrary geometry, thermoelastic interaction, and gaps. It is possible to model any inner race, outer race, and housing desired, but accurate calculation of rolling element kinematics is difficult. On the other hand, bearing mechanics software has been well developed for many years, but does not include general race compliance and deadband effects. The logical new approach outlined below augments the bearing mechanics software with a full stiffness representation of the hardware derived from finite element analysis. The existing capability to analyze detailed kinematics, Hertzian contact, and centrifugal loading is used with minor modification.

Modification of Contact Algorithms

The nonlinear equations governing bearing mechanics are commonly solved by Newton-Raphson methods as follows:

1. Guess bearing race rigid body relative deflections.
2. Compute resultant ball deflections and loads by kinematic and Hertzian contact equations.
3. Compare the vector sum of ball loads to given external loads. The difference is error loads.
4. Convert load errors to incremental displacements using an updated linear compliance based on current ball loading (tangent compliance).
5. Return to 2. with new displacements until convergence.

Inclusion of flexibility/deadband effects can be achieved by appropriate modification of step 2, ball load calculation, and step 4, linear compliance calculation. In the new method, the ball loads from step 2, which act equal and opposite on the races, are used to compute race deflections r_{oj}, z_{oj}, r_{ij}, z_{ij}, at the contact points of each ball j (subscripts o, i indicate outer and inner race). These deflections are returned to step 2, along with the updated total relative rigid body deflections δ_x, δ_y (along external radial loads), δ_a (axial), and θ_x, θ_y (angular about external moment axes). The rigid body motions require conversion to individual relative race motions Δr_j, Δz_j, at each ball. Given rigid body radii to raceway curvature centers $\mathscr{R}_o$ and $\mathscr{R}_i$, and ball j azimuth angle from the x direction ψ_j, the individual ball rigid body motions are, [2],

$$\Delta r_j = \delta_x \cos\psi_j + \delta_y \sin\psi_j \tag{2a}$$

$$\Delta z_j = \delta_a + \mathscr{R}_i \theta_x \sin\psi_j - \mathscr{R}_i \theta_y \cos\psi_j \tag{2b}$$

The actual deflections seen by the ball are less than these values due to race compliance motions,

$$\Delta r_{bj} = \Delta r_j - r_{oj} + r_{ij} \tag{3a}$$

$$\Delta z_{bj} = \Delta z_j - z_{oj} + z_{ij} \tag{3b}$$

Note that cylindrical coordinates are assumed for all race deflections, with positive sense outward for r and in the direction of positive axial loading for z.

As Figure 3 shows for the race flexure case, the variables A_{1j} and A_{2j} used in solving the nonlinear equations, [2], can now be redefined as

$$A_{1j} = BD\sin\alpha^\circ + \Delta z_j - z_{oj} + z_{ij} \tag{4a}$$

$$A_{2j} = BD\cos\alpha^\circ + \Delta r_j - r_{oj} + r_{ij} \tag{4b}$$

while the definitions of X_{1j}, X_{2j} are unchanged by the flexure, [2],

$$X_{1j} = [\,(f_o - 0.5)D + \delta_{oj}\,]\sin\alpha_{oj} \tag{5a}$$

$$X_{2j} = [\,(f_o - 0.5)D + \delta_{oj}\,]\cos\alpha_{oj} \tag{5b}$$

See Harris [2] Chapter 8.3 and 8.6 for details of the subsequent ball load solution using A_{1j}, A_{2j}, X_{1j}, X_{2j}.

Actual computation of the current race flexure r_{oj}, z_{oj}, r_{ij}, z_{ij} is straightforward if bearing race compliance matrices are available for the current ball load levels. Incremental deflections are computed using incremental ball load by

$$\begin{bmatrix} \vdots \\ \Delta r_{oj} \\ \Delta z_{oj} \\ \vdots \end{bmatrix} = \mathbf{C}_o(Q_{oj}) \qquad \begin{bmatrix} \vdots \\ \Delta Q_{oj}\cos\alpha_{oj} \\ \Delta Q_{oj}\sin\alpha_{oj} \\ \vdots \end{bmatrix} = \mathbf{C}_o\Delta\mathbf{F} \tag{6}$$

and added to the deflections from the previous iteration (similarly for the inner race). Generation of the race compliance matrix $\mathbf{C}_o$ will be discussed later. First, consider step 4 of the solution augmented by this new compliance. The race compliances are in series with the ball compliances, and both vary with ball load. Consider the outer race contact relation, [2],

$$Q_{oj} = K_{oj}\delta_{oj}^{3/2} \tag{7}$$

which can be broken into r and z components by noting

$$Q_{orj} = Q_{oj}\cos\alpha_{oj} \quad \text{and} \quad \delta_{orj} = \delta_{oj}\cos\alpha_{oj} \tag{8a}$$

$$Q_{ozj} = Q_{oj}\sin\alpha_{oj} \quad \text{and} \quad \delta_{ozj} = \delta_{oj}\sin\alpha_{oj} \tag{8b}$$

The result in r and z compliance form is

$$\delta_{orj} = \frac{\cos^{1/3}\alpha_{oj}}{K_{oj}^{2/3}}\, Q_{orj}^{2/3} \tag{9a}$$

$$\delta_{ozj} = \frac{\sin^{1/3}\alpha_{oj}}{K_{oj}^{2/3}}\, Q_{ozj}^{2/3} \tag{9b}$$

Linearized tangent compliance at the current Q_{oj} can be obtained by taking the partials of (9) with respect to Q_{orj}, Q_{ozj}. This is greatly simplified by assuming α_{oj} constant, which is reasonable for small load increments. The compliance is then

$$c_{orj} = \frac{\partial \delta_{orj}}{\partial Q_{orj}} = \frac{2}{3K_{oj}^{2/3} Q_{oj}^{1/3}} = c_{oj} \tag{10a}$$

$$c_{ozj} = \frac{\partial \delta_{ozj}}{\partial Q_{ozj}} = \frac{2}{3K_{oj}^{2/3} Q_{oj}^{1/3}} = c_{oj} \tag{10b}$$

These ball compliances, with similar results for the inner race contact, can be summed with the race compliances to give approximate total bearing tangent compliance in individual ball terms of

$$\mathbf{C} = \mathbf{C}_o(Q_{oj}) + \mathbf{C}_i(Q_{ij}) + \begin{bmatrix} \ddots & & \\ & c_{oj} & \\ & & c_{oj} \end{bmatrix} + \begin{bmatrix} \ddots & & \\ & c_{ij} & \\ & & c_{ij} \end{bmatrix} \tag{11}$$

$\mathbf{C}$ can then be used to determine the incremental rigid body displacements δ_x, δ_y, δ_a, θ_x, θ_y, due to load error by using constraint matrices constructed as follows. With multiple applications of equations (2), the conventional (Reference [2]) kinematic relationship can be written in matrix form,

$$\Delta \mathbf{x} = \Lambda_\delta \, \boldsymbol{\delta} \tag{12}$$

where

$$\Delta \mathbf{x}^T = [\bullet\bullet\bullet \, \Delta r_j \; \Delta z_j \, \bullet\bullet\bullet] \tag{13a}$$

$$\boldsymbol{\delta}^T = [\, \delta_x \; \delta_y \; \delta_a \; \theta_x \; \theta_y \,] \tag{13b}$$

and $\Delta \mathbf{x}$ and $\boldsymbol{\delta}$ are now defined to be incremental quantities for the current external load error, and

$$\Lambda_\delta = \begin{bmatrix} & & \vdots & & \\ \cos\psi_j & \sin\psi_j & 0 & 0 & 0 \\ 0 & 0 & 1 & \mathscr{R}_i \sin\psi_j & -\mathscr{R}_i \cos\psi_j \\ & & \vdots & & \end{bmatrix} \tag{14}$$

By definition of the compliance matrix $\mathbf{C}$,

$$\Delta \mathbf{x} = \mathbf{C} \, \Delta \mathbf{F}_x \tag{15}$$

where

$$\Delta \mathbf{F}_x^T = [\bullet\bullet\bullet \, \Delta Q_{irj} \; \Delta Q_{izj} \, \bullet\bullet\bullet] \tag{16}$$

are individual ball load errors. The summation of ball load errors gives the external load error, and can be written in matrix form as

$$\Delta \mathbf{F}_\delta = \Lambda_F^T \, \Delta \mathbf{F}_x \tag{17}$$

where

$$\Lambda_F = \begin{bmatrix} \vdots & & & & \\ \cos\psi_j & \sin\psi_j & 0 & -\ell_{2j}\sin\psi_j & \ell_{2j}\cos\psi_j \\ 0 & 0 & 1 & \ell_{1j}\sin\psi_j & -\ell_{1j}\cos\psi_j \\ \vdots & & & & \end{bmatrix} \tag{18}$$

ℓ_{1j} and ℓ_{2j} are ball load lever arms about the load application point on the inner race,

$$\ell_{1j} = \mathscr{R}_i - f_i D\cos\alpha_{ij} \tag{19a}$$

$$\ell_{2j} = \mathscr{Z}_i - f_i D\sin\alpha_{ij} \tag{19b}$$

where $\mathscr{Z}_i$ is the constant axial distance from the load point to the plane containing the inner raceway curvature center locus. The effect of inner race deflection on ℓ_{1j} and ℓ_{2j} is negligible.

Inverting (15), and using (12) and (17) yields the compliance relationship in terms of rigid body incremental deflections,

$$\delta = [\Lambda_F^T \mathbf{C}^{-1} \Lambda_\delta]^{-1} \Delta\mathbf{F}_\delta \tag{20}$$

Note that the matrix computation of Λ_F must be performed in each iteration unless one is willing to neglect the varying terms.

Although some approximations are made in the foregoing (θ_x, θ_y small, for example), the result (20) is of sufficient accuracy to ensure good Newton-Raphson incrementation and convergence. Absolute accuracy is not critical in the Newton-Raphson compliance update steps. The total ball load summation, however, must be accurate to obtain a correct solution, i.e., the load balance must be correct on the inner race. Equation (17) should be used for this purpose. Conventional bearing mechanics programs use $\ell_{1j} = d_m/2$ and $\ell_{2j} = 0$ which is convenient because Λ_F becomes constant, but is not strictly correct. Such an approximation neglects moment due to radial ball loads as well as lever arm changes with contact angle.

Bearing Race/Housing Models

The calculation of $\mathbf{C}_o$ and $\mathbf{C}_i$ required for equations (6) and (11) can be handled as a separate process within each Newton-Raphson iteration. The four types of bearing/housing configurations of interest are the following:

KL0: flexible inner race.
KL1: flexible outer race and housing with no deadband.
KL2: flexible outer race with deadband, and housing assumed rigid.
KL3: flexible outer race and housing with deadband.

All of these types are amenable to general finite element modeling such as that shown in Figures 4 and 5 with balls omitted. The models need not be symmetric, and can be subjected to thermal loads, interference fits, and so on within the finite element program. The finite element models can be substructured (static condensation) in cylindrical coordinates to only degrees of freedom (DOFs) at nominal ball contact points and gap interfaces. Figure 6 shows the DOFs of interest for each configuration type, and the unloaded reduced stiffness matrix form. The choice of gap interface location and number is left to the analyst.

To ensure invertibility of $\mathbf{K}_o$, it is necessary to add soft springs across enough gaps within the finite element model to restrain rigid body motion (indicated by ε_{oh}, ε_{rh}). The springs should be just soft enough to produce negligible load at gap closure. Similarly, invertibility of $\mathbf{K}_i$ requires soft springs from several ball

contact points to ground. These springs should be several orders of magnitude softer than the expected bearing stiffness, so that they generate negligible loads. With invertibility assured, the total compliance matrices are

$$\text{KL0: } \mathbf{K}_i^{-1} = [\mathbf{C}_i] \tag{21a}$$

$$\text{KL1: } \mathbf{K}_o^{-1} = [\mathbf{C}_o] \tag{21b}$$

$$\text{KL2: } \mathbf{K}_o^{-1} = \begin{bmatrix} \mathbf{C}_o & \mathbf{C}_{or} \\ \mathbf{C}_{or} & \mathbf{C}_{rr} \end{bmatrix} \tag{21c}$$

$$\text{KL3: } \mathbf{K}_o^{-1} = \begin{bmatrix} \mathbf{C}_o & \mathbf{C}_{or} & \mathbf{C}_{oh} \\ \mathbf{C}_{or} & \mathbf{C}_{rr} & \mathbf{C}_{rh} \\ \mathbf{C}_{oh} & \mathbf{C}_{rh} & \mathbf{C}_{hh} \end{bmatrix} \tag{21d}$$

where the partitions $\mathbf{C}_i$ and $\mathbf{C}_o$ are the matrices needed for equations (6) and (11).

During solution iterations, the incremental race deflections are computed using equation (6) with $\mathbf{C}_i$ or $\mathbf{C}_o$ from above and the current ball incremental loading. First, $\mathbf{K}_o^{-1}$ must be iteratively modified to account for gap closure or opening. The gap interface deflections must be checked by evaluating the increments, which are computed using current ball incremental loading $\Delta\mathbf{F}$

$$\Delta\mathbf{x}_r - \Delta\mathbf{x}_h = (\mathbf{C}_{or} - \mathbf{C}_{oh})\,\Delta\mathbf{F} \tag{22}$$

since the ball loads are the only external loads on the race. The increments are then added to the previous gap deflections, and the totals are compared to the specified gap sizes. If a gap has closed, then $\mathbf{K}_o$ must be augmented by a high stiffness across the gap which can be represented in the matrix form as

$$\begin{bmatrix} F_{rk} \\ F_{zk} \\ -F_{rk} \\ -F_{zk} \end{bmatrix} = \begin{bmatrix} k_r & 0 & -k_r & 0 \\ 0 & k_z & 0 & -k_z \\ -k_r & 0 & k_r & 0 \\ 0 & -k_z & 0 & k_z \end{bmatrix} \begin{bmatrix} r_{rk} \\ z_{rk} \\ r_{hk} \\ z_{hk} \end{bmatrix} \tag{23}$$

Similarly, an opened gap requires augmentation with the negative of above. A new $\mathbf{K}_o^{-1}$ is computed and the gap checking process is repeated until no gaps change. Then the resulting $\mathbf{C}_o$ can be used in equations (6) and (11). Excessively large values of k_r and k_z can cause solution instability, and should be avoided. A good scheme to determine these values is to find the largest term in the unloaded $\mathbf{K}_o$ and multiply that by 100 to 1000. It is prudent to check the conditioning of $\mathbf{K}_o^{-1}$ during the analysis and adjust k_r, k_z as required.

Combined Analysis

The overall analysis can now be summarized by the following steps. Steps that are new are highlighted in bold.

1. Supply "rigid" bearing dimensions, parameters and loads, to bearing mechanics program.

2. Read race matrices $\mathbf{K}_i$ and $\mathbf{K}_o$ into program, along with gap size list.

3. Perform first iteration using race rigidity assumption to obtain ball loads.

4. Compute race deflections by equation (6).

5. Recalculate ball loads using existing code modified by equations (4).

6. Check resultant load errors using the more exact equation (17). If negligible, stop.

7. Update tangent compliance of outer race using $\mathbf{K}_o$ and equations (22), (23) in an iterative loop, given incremental ball loads for this iteration.

8. Compute incremental race deflections by equation (6), given incremental ball loads and updated race compliance.

9. Update total tangent compliance **C** and incremental rigid body motion δ using equations (10), (11), (19), and (20).

10. Return to **5.** with all updated displacements (previous + increments), both rigid body and flexural. This allows determination of A_{1j}, A_{2j}.

Note that since steps 7 and 8 use incremental ball loads for the current iteration and not for the total load error in step 6, the compliance corrections and race deflections lag the Newton-Raphson update. Unfortunately, it is not possible to uniquely determine the individual ball load errors due to total load error in step 6. An approximate determination of $\Delta\mathbf{F}_X$ could be made by using a least squares estimate of equation (17) given $\Delta\mathbf{F}_\delta$ load errors. However, the improvement in Newton-Raphson convergence would be offset by the least squares computations required. For now, the least squares estimation is omitted.

BEARING PRELOADING ANALYSIS

The case of axial loading only at zero speed (preloading) greatly simplifies the computations discussed. All contact angles become equal for a symmetric bearing, radial and moment load resultant are zero, and all balls behave the same given a symmetric race model. The simplified versions of the general equations presented are easily incorporated into existing bearing mechanics software. The sample analysis shown below was performed using an augmented version of the readily available bearing mechanics program developed by A.B. Jones. The new program has been named ROBEAN (ROlling BEaring ANalysis).

The Bearing Model

The bearing described in Table 1 was used for the sample preloading analysis. Figure 4 shows the outer race model. The inner race was assumed rigid. Figure 5 shows a schematic of the gaps at each ball and race restraint used. In addition, very soft springs of 17,520 N/m (100 lb/in) span the gaps in r and z cylindrical directions, and for the KL3 flexible housing case, the housing is represented by 1.75×10^8 N/m (1.0×10^6 lb/in) springs in r and z at each gap. The reduced stiffness matrices for cases KL1, KL2, and KL3 were prepared with ANSYS and read into ROBEAN automatically. Uniform gap values of 0.0050 mm (0.0002 in) were also supplied for KL2 and KL3. Additionally, the usual "rigid" bearing inputs were entered as always.

Results

Preloads of up to 8900 N (2000 lb) were applied to the bearing in ROBEAN, for the three cases KL1, KL2, and KL3. A fourth case where gaps never close was also included for comparison after gap closure of KL2 and KL3. Results from Harris [2], Chapter 6.5, assuming rigid races are presented with the new results in Figures 7 and 8.

The results show the differences in axial deflection and contact angle for the different bearing types studied. In both figures, the nonlinear variations with preload can be seen. Only Hertzian contact at the ball/race interfaces is accounted for in the Harris calculations. Therefore, this bearing model shows the greatest stiffness in Figure 7. The KL1 bearing model adds outer race bulk flexibility, and its effective

stiffness is slightly less. Note that the Hertzian deformations already included in the ball load calculations do not occur in the finite element model because of its mesh coarseness. If they had, KL1 stiffness would be much less.

The KL2 bearing accounts for a radial gap clearance of 0.0050 mm (0.0002 in). A significant decrease in axial stiffness is seen for this bearing before gap closure in comparison to the rigid model. This is due to the unrestrained growth of the outer race. Approximately 5120N (1150 lb) of preload is needed to close the gap. At gap closure, KL2 bearing stiffness is increased, and now essentially matches that of the KL1 case. However, total axial deffection is greater.

The KL3 bearing stiffness is essentially equivalent to KL2 up to the point of gap closure. The extra housing compliance results in a smaller stiffness increase upon gap closure than the KL2 case.

CONCLUSIONS

1. New accurate methods have been developed to include arbitrary race/housing/deadband structures in bearing loading analysis. The flexible structures except balls and Hertizian contact are modeled and substructured using available finite element programs. The effects can be included within existing Newton-Raphson bearing mechanics program iterations with minimal impact.

2. The new methods are shown to be viable for a preloading example. Axial stiffness is significantly affected by outer race clearance.

3. The preloading example results indicate a need to investigate more complex loading cases. The authors will do so and present results in another paper.

4. Although not specifically discussed, the analyst's freedom of gap modeling implicitly allows the new methods to account for general outer race misalignment or "cocking" within the housing bore, including full flexibility and nonuniform geometry effects. This only requires more gaps to be defined, and the formulation is unchanged.

5. The following effects have been neglected in the development presented, and are still under investigation by the authors:

   - contact angle change due to flexure and "cocking" induced local rotation only - likely negligible, because such rotations are much smaller than the contact angle changes.
   - change in $\mathscr{R}_i, \mathscr{R}_o$, raceway curvature, and other size parameters due to flexure - likely negligible, because flexural changes are small percentage of nominal.
   - change in race stiffness due to movement of contact point on the race - possibly non-negligible, because movement is significant, proportional to contact angle change.

REFERENCES

1. Jones, A.B., A General Theory of Elastically Constrained Ball and Radial Roller Bearings Under Arbitrary Load and Speed Conditions, *ASME J. of Basic Engineering*, vol. 82, Series D, pp. 309-320, June 1960.

2. Harris, T.A., *Rolling Bearing Analysis*, 2nd Edition, John Wiley & Sons, New York, 1984.

3. Kleckner, R.J., Pirvics, J., and Castelli, V., High Speed Cylindrical Rolling Element Bearing Analysis "CYBEAN" - Analytic Formulation, *ASME J. of Lubrication Technology*, vol. 102, pp. 380-390, July 1980.

4. Childs, D.W. and Moyer, D.S., Vibration Characteristics of the HPOTP (High Pressure Oxygen Turbopump) of the SSME (Space Shuttle Main Engine), ASME paper #84-GT-31, presented at the *29th International Gas Turbine Conference and Exhibit, Amsterdam*, 8 pg , June 1984.

5. Cody, J.C. et. al., Bearing Tester Data Compilation, Analysis, and Reporting and Bearing Math Modeling, Final Report, Volume 1, by Spectra Research Systems for NASA/MSFC, contract no. NAS8-34686, NASA CR-171039, 137 pg, May 1984.

6. Beatty, R.F. and Rowan, B.F., Determination of Ball Bearing Dynamic Stiffness, in *Rotordynamic Instability Problems in High-Performance Turbomachinery - 1982,* Proceedings of a Workshop held at College Station, Texas, pp. 98-104, May 10-12, 1982. NASA CR-2250 .

TABLE 1. Subject bearing specification

Bore	:	45 mm (1.771 in)
Number of Balls	:	14
Ball Diameter	:	8.74 mm (.344 in)
Pitch Diameter	:	59.44 mm (2.34 in)
Unmounted Contact Angle	:	18.24°
Outer Raceway Osculation	:	.523
Inner Raceway Osculation	:	.532

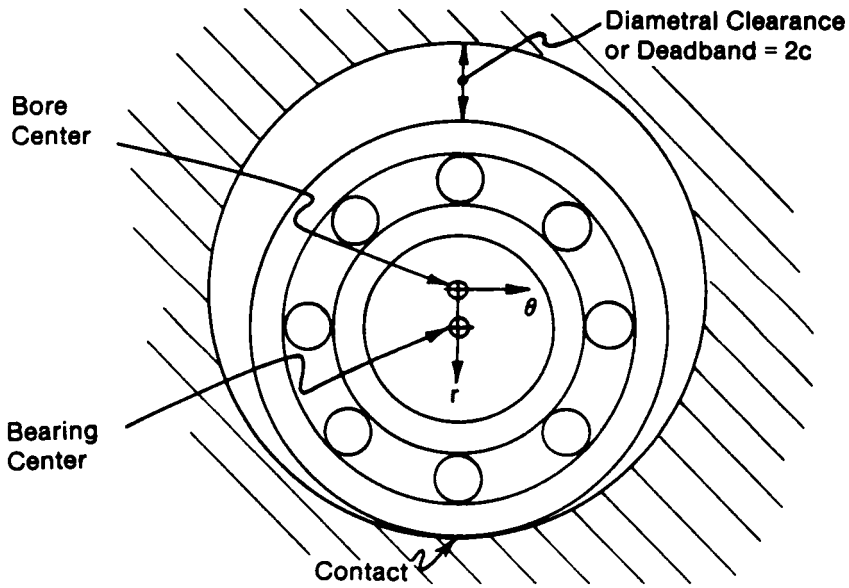

FIGURE 1. A bearing with deadband, unloaded

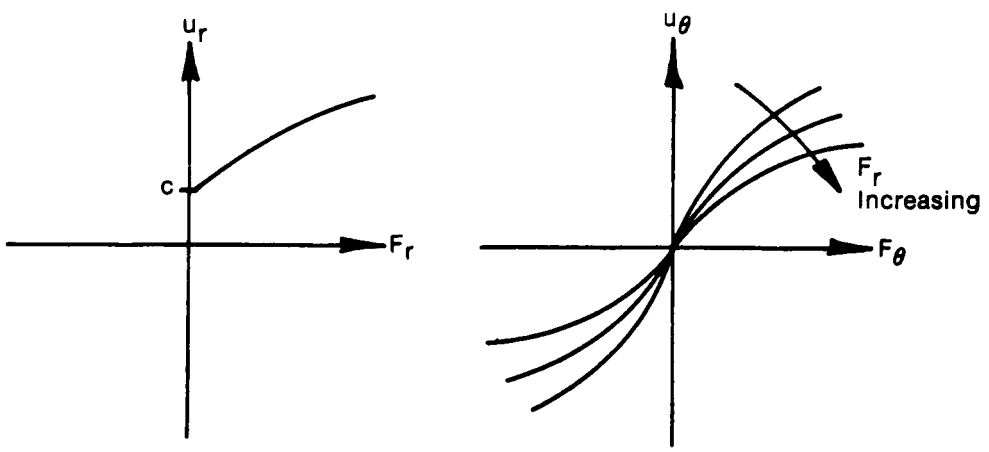

FIGURE 2. General load-deflection relationships for a flexible bearing with deadband

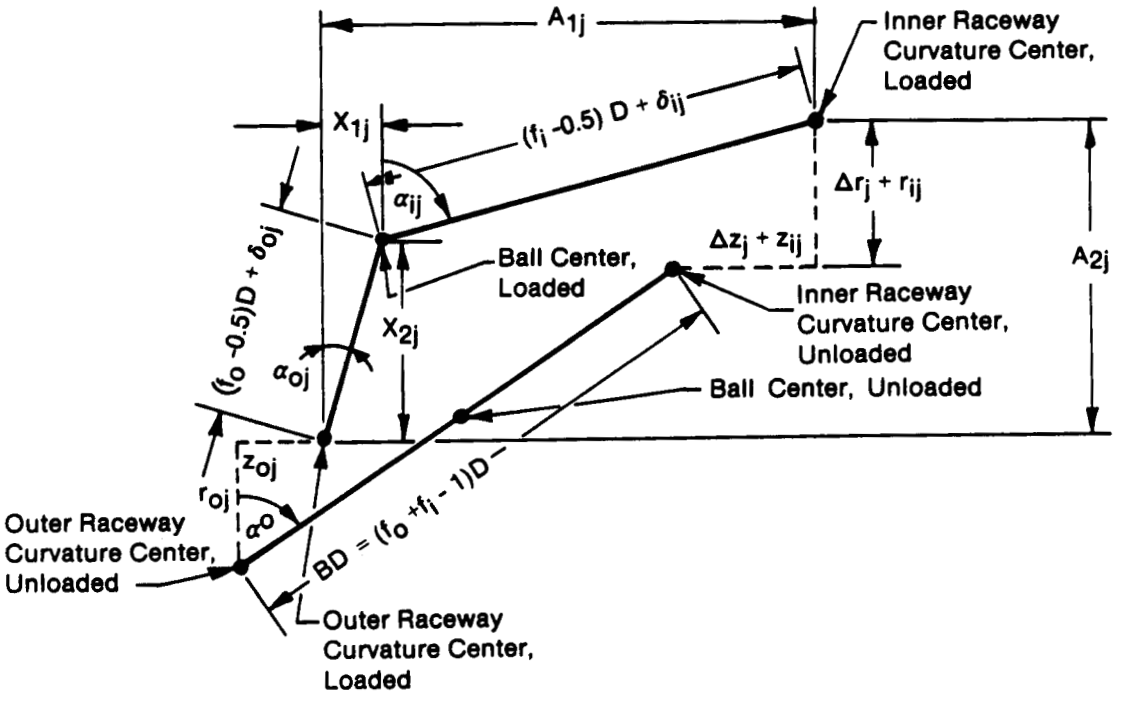

FIGURE 3. Ball bearing kinematics including race flexure

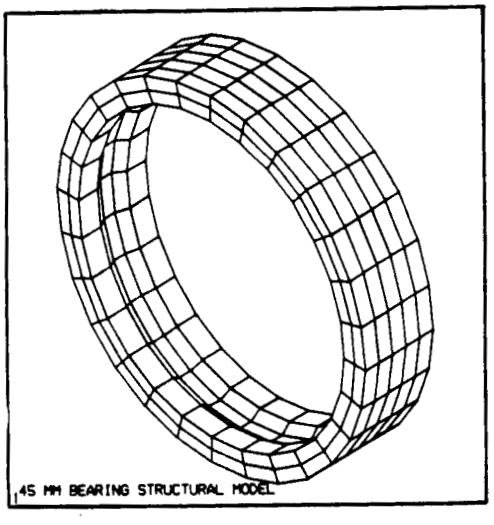

FIGURE 4. Outer race finite element model

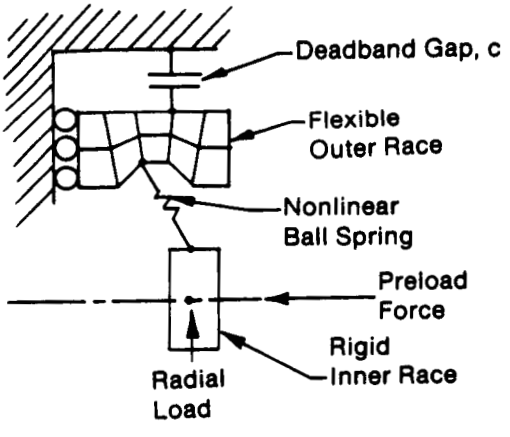

FIGURE 5. Bearing model schematic

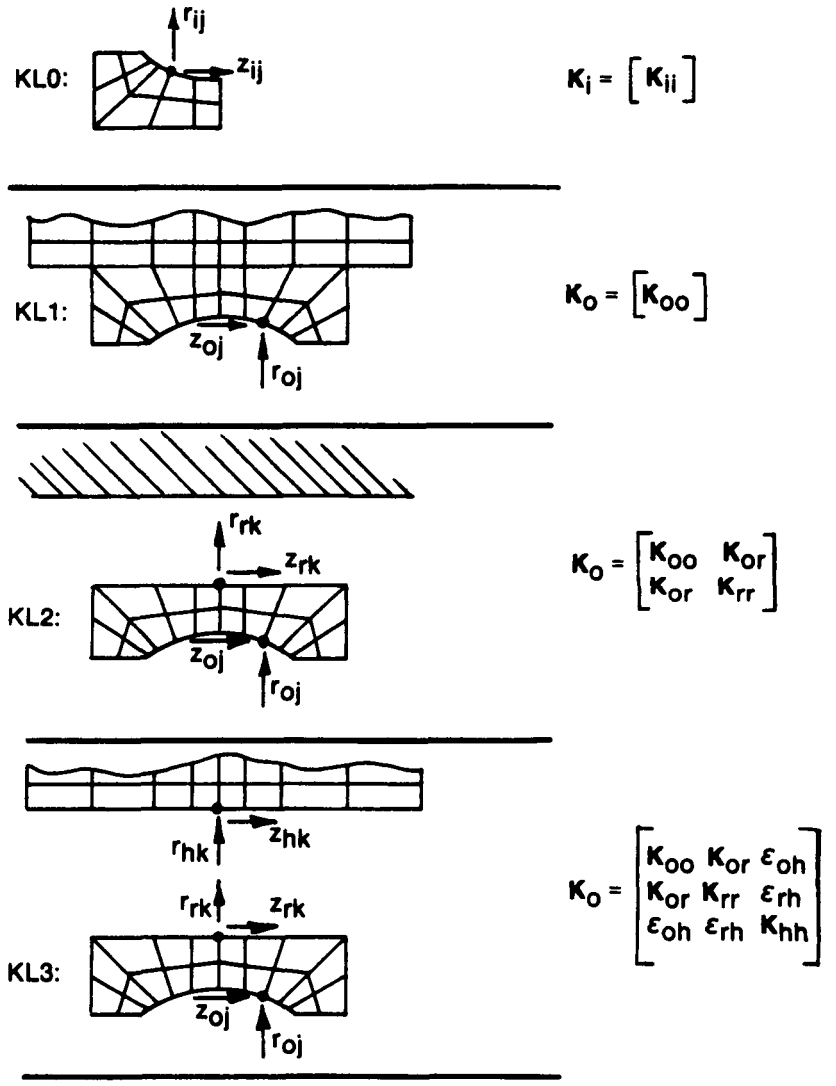

FIGURE 6. DOFs of interest in race/housing models

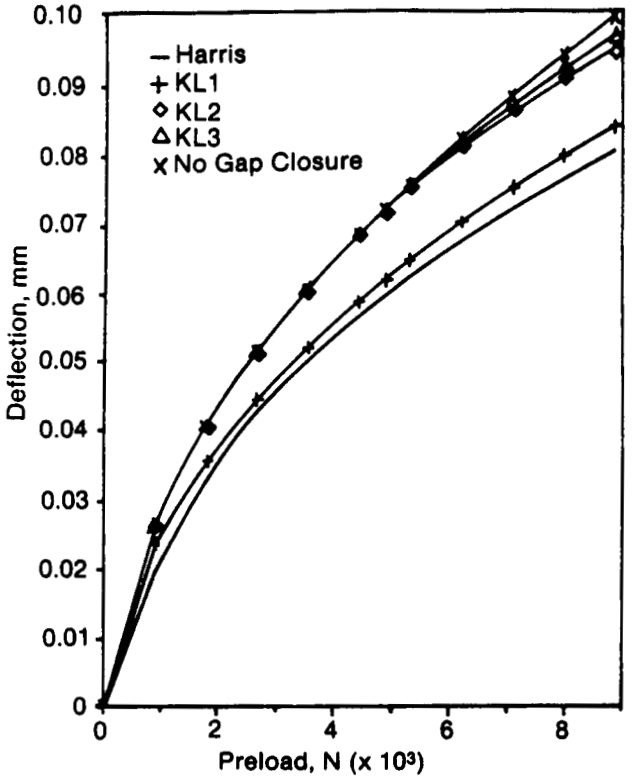

FIGURE 7. Axial deflection vs. preload for the various bearing types

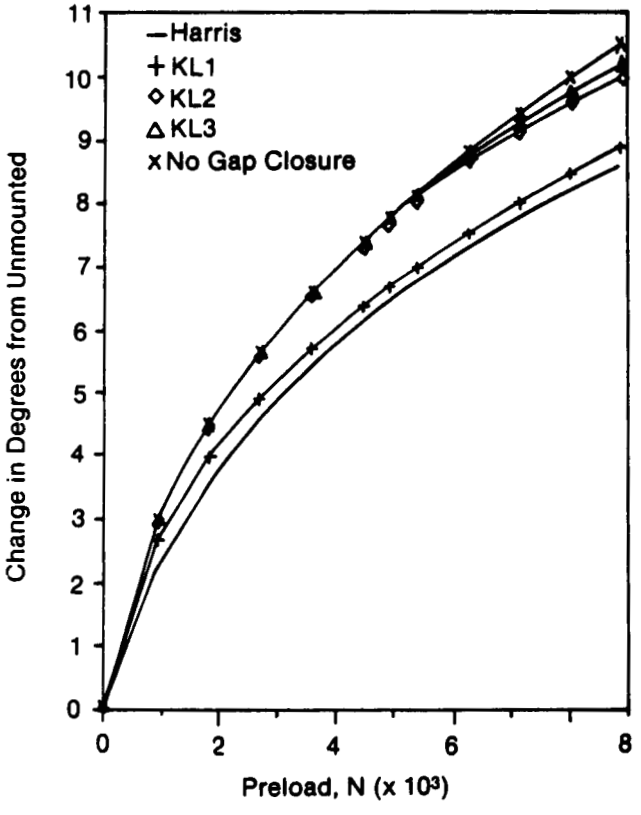

FIGURE 8. Change in contact angle vs. preload for the various bearing types